J|A|C|S
ARTICLES
Published on Web 03/24/2006

Probing Methyl Dynamics from ^{13}C Autocorrelated and Cross-Correlated Relaxation

Xu Zhang,[†,‡] Xiaogang Sui,[§] and Daiwen Yang*[,†]

Contribution from the Department of Biological Sciences, National University of Singapore, 14 Science Drive 4, Singapore 117543, State Key Laboratory of Magnetic Resonance and Molecular and Atomic Physics, Wuhan Institute of Physics and Mathematics, The Chinese Academy of Sciences, Wuhan, 430071, PR China, and Department of Chemistry, National University of Singapore, 14 Science Drive 4, Singapore 117543

Received November 7, 2005; E-mail: dbsydw@nus.edu.sg

Abstract: An understanding of side-chain motions in protein is of great interest since side chains often play an important role in protein folding and intermolecular interactions. A novel method for measuring dipole−dipole cross-correlated relaxation in methyl groups of uniformly ^{13}C-labeled proteins without deuteration has been developed by our group. The excellent agreement between dynamic parameters of methyl groups in ubiquitin obtained from the cross-correlated relaxation and ^{13}C spin−lattice relaxation and those derived previously from ^{2}H relaxation data demonstrates the reliability of the method. This method was applied to the study of side-chain dynamics of human intestinal fatty acid binding protein (IFABP) with and without its ligand. Binding of oleic acid to the protein results in decreased mobility of most of the methyl groups in the binding region, whereas no significant change in mobility was observed for methyl groups in the nonbinding region.

Introduction

The dynamic aspects of macromolecules are increasingly recognized as important for describing their biological functions.[1−4] As a consequence, considerable effort has been made to characterize protein dynamic motions, mainly from NMR relaxation,[5−8] amide proton exchange studies,[9] fluorescence spectroscopy,[10] molecular dynamics simulations,[11] and X-ray studies.[12]

Up to now, relaxation studies of proteins on fast motions have concentrated primarily on backbone dynamics. However, an understanding of protein side-chain motions is of potentially greater interest.[13−18] Methyl groups are a particularly good target for dynamics studies since they are often found in the hydrophobic cores of proteins and their motion is essential for protein folding, stability, ligand binding, and protein−protein interaction.[19−21] Unlike backbone amides, which are considered as isolated two-spin systems, methyl and methylene groups (CH_3 and CH_2) in uniformly ^{13}C-labeled proteins suffer from $^{13}C-^{13}C$ J coupling and cross-correlated relaxation between C−H dipoles in the measurement of ^{13}C transverse relaxation time. Thus the methods used for backbone ^{15}N spins cannot be applied to side-chain ^{13}C spins. Currently, methyl dynamics on a nanosecond-to-picosecond time scale are obtained mainly from the relaxation data of a deuteron in CH_2D methyl groups of ^{13}C-labeled, fractionally deuterated proteins, which are made for the sole purpose of deuterium relaxation studies.[13,22,23] Measurement of deuterium relaxation requires ^{2}H-decoupling hardware and calibration of a ^{2}H pulse that are not used in most structure studies and are unfamiliar to many spectroscopists. In principle, methyl dynamics can be extracted from ^{13}C relaxation time T_1 and a heteronuclear NOE measured at multiple static

[†] Department of Biological Sciences, National University of Singapore.
[‡] The Chinese Academy of Sciences.
[§] Department of Chemistry, National University of Singapore.

(1) Ilangovan, U.; Ding, W.; Zhong, Y.; Wilson, C. L.; Groppe, J. C.; Trbovich, J. T.; Zuniga, J.; Demeler, B.; Tang, Q.; Gao, G.; Mulder, K. M.; Hinck, A. P. *J. Mol. Biol.* **2005**, *352*, 338−54.
(2) Finerty, P.; Mittermaier, A.; Muhandiram, R.; Kay, L. E.; Forman-Kay, J. D. *Biochemistry* **2005**, *44*, 694−703.
(3) Onuchic, J. N.; Luthey-Schulten, Z.; Wolynes, P. G. *Annu. Rev. Phys. Chem.* **1997**, *48*, 545−600.
(4) Dutta, K.; Shi, H.; Cruz-Chu, E. R.; Kami, K.; Ghose, R. *Biochemistry* **2004**, *43*, 8094−106.
(5) Kay, L. E. *J. Magn. Reson.* **2005**, *173*, 193−207.
(6) Nesmelova, I.; Krushelnitsky, A.; Idiyatullin, D.; Blanco, F.; Ramirez-Alvarado, M.; Daragan, V. A.; Serrano, L.; Mayo, K. H. *Biochemistry* **2001**, *40*, 2844−2853.
(7) Palmer, A. G. *Annu. Rev. Biophys. Biomol. Struct.* **2001**, *30*, 129−155.
(8) Akke, M. *Curr. Opin. Struct. Biol.* **2002**, *12*, 642−647.
(9) Loh, S. N.; Wang, J.; Markley, J. L. *Biochemistry* **1993**, *32*, 11022−11028.
(10) Palmer, A. G.; Millar, D. P.; Rance, M.; Wright, P. E. *J. Am. Chem. Soc.* **1993**, *115*, 6333−6345.
(11) Smith, L. J.; Mark, A. E.; Dobson, C. M.; Gunsteren, W. F. v. *Biochemistry* **1995**, *34*, 10918−31.
(12) Buck, M.; Boyd, J.; Redfield, C.; MacKenzie, D. A.; Jeenes, J. D.; Archer, D. B.; Dobson, C. M. *Biochemistry* **1995**, *34*, 4041−55.
(13) Muhandiram, D. R.; Yamazaki, T.; Sykes, B. D.; Kay, L. E. *J. Am. Chem. Soc.* **1995**, *117*, 11536−11544.
(14) LeMaster, D. M.; Kushlan, D. M. *J. Am. Chem. Soc.* **1996**, *118*, 9255−64.
(15) Engelke, J.; Rüterjans, H. *J. Biomol. NMR* **1998**, *11*, 165−183.
(16) Houben, K.; Boelens, R. *J. Biomol. NMR* **2004**, *29*, 151−166.
(17) Yang, D. W.; Mittermaier, A.; Mok, Y. K.; Kay, L. E. *J. Mol. Biol.* **1998**, *276*, 939−954.
(18) Zheng, Y.; Yang, D. W. *J. Biomol. NMR* **2004**, *28*, 103−116.
(19) Lee, A. L.; Kinnear, S. A.; Wand, A. J. *Nat. Struct. Biol.* **2000**, *7*, 72−77.
(20) Ishima, R.; Torchia, D. A. *Nat. Struct. Biol.* **2000**, *7*, 740−743.
(21) Goehlert, V. A.; Krupinska, E.; Regan, L.; Stone, M. J. *Protein Sci.* **2004**, *13*, 3322−30.
(22) Millet, O.; Muhandiram, D. R.; Skrynnikov, N. R.; Kay, L. E. *J. Am. Chem. Soc.* **2002**, *124*, 6439−6448.
(23) Skrynnikov, N. R.; Millet, O.; Kay, L. E. *J. Am. Chem. Soc.* **2002**, *124*, 6449−60.

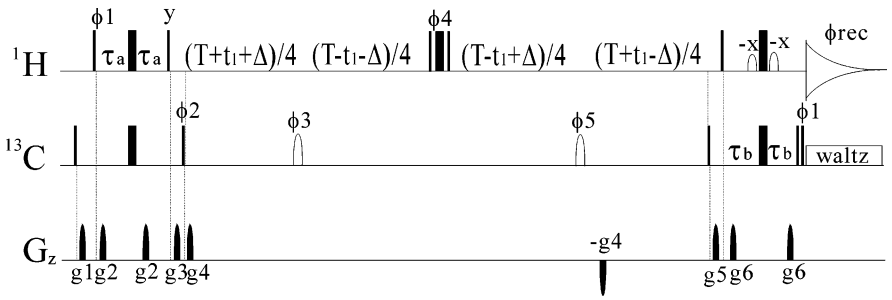

Figure 1. Pulse scheme for the measurement of dipole−dipole cross-correlated relaxation in methyl groups of uniformly ^{13}C, ^{15}N-labeled proteins. The carriers are centered at 4.7 and 19 ppm for ^{1}H and ^{13}C, respectively. Narrow and wide bars correspond to 90° and 180° RF pulses, respectively. The unfilled ^{1}H shapes are rectangular 90° pulses (1.2 ms). The ^{13}C shaped 180° pulses have an REBURP profile (300 μs, centered at 38 ppm, bandwidth ±6.7 kHz). The value of T is set to n/J_{CC}, where n is an integer. Delays used are $\tau_a = 1$ ms and $\tau_b = 1.95$ ms. The phase cycling used is: $\phi_1 = 4(x), 4(-x)$; $\phi_2 = x$; $\phi_3 = x, y, -x, -y$; $\phi_4 = 2(x), 2(-x)$; $\phi_5 = 2(x), 2(y), 2(-x), 2(-y)$; $\phi_{rec} = x\ -x\ -x\ x\ -x\ x\ x\ -x$. The duration and amplitude of the sine-shaped gradients are: g1 = (1 ms, 7.5 G/cm); g2 = (0.5 ms, 15 G/cm); g3 = (2 ms, 24 G/cm); g4 = (1 ms, 15 G/cm); g5 = (1 ms, 10 G/cm); g6 = (0.5 ms, 30 G/cm). Quadrature detection in the F_1 dimension is achieved by the states-TPPI of phase ϕ_2.

magnetic fields.[24] However, order parameters obtained with this method are error-prone because both T_1 and NOE are insensitive to methyl order parameters, especially for larger proteins. If a specifically labeled sample with $^{12}C-^{13}CHD_2$ labeling patterns is available, methyl dynamics can be probed with ^{13}C relaxation data (T_1, T_2, and NOE),[14,25] which is measured and analyzed in a manner similar to amide dynamics.

Recently, we have shown that side-chain dynamics can be estimated from dipole−dipole cross-correlated relaxation using uniformly ^{13}C,^{15}N-labeled proteins.[18,26] However, the methods are limited to proteins smaller than ∼15 kDa. Here, we present a simple novel method for obtaining methyl dynamics from ^{13}C spin−lattice relaxation rates (R_1) and dipole−dipole cross-correlated relaxation rates (Γ). The cross-correlated relaxation rates are measured from a sensitive 2D HSQC-based experiment. The method is demonstrated on ubiquitin (UB) and applied to the study of side-chain dynamics of human intestinal fatty acid binding protein (IFABP) in the presence and absence of ligand.

Fatty acid binding proteins constitute a family of small (∼15 kDa) proteins with considerable variation in amino acid sequence yet similar three-dimensional structures in different tissues.[27] They are found in cytosol of various tissues and organs, such as intestinal mucosa, liver, myocardium, adipose tissue, kidney, and aid in translocating and storing long-chain fatty acids and certain other lipids.[28] Intestinal fatty acid binding protein (IFABP) is a member of this family of proteins. X-ray structures indicate only very small conformational differences between ligand free and bound IFABPs.[29] Solution NMR structures show that the portal region in the fatty acid free form is less ordered and is considered as the entry to the ligand.[30] Backbone NMR relaxation studies reveal backbone dynamics of apo- and holo-forms as very similar,[31] except for residues in the portal region. Side-chain dynamics reported here will serve as the first step to understanding the binding specificity, affinity, and mechanism of ligand entry and exit.

Materials and Methods

NMR Spectroscopy. All NMR experiments were performed on a Bruker Avance 800 MHz spectrometer. The experiments for UB were recorded on a sample of uniformly ^{13}C, ^{15}N-labeled protein (∼1 mM, pH 6.5, 75 mM phosphate, 10% D_2O, 27 °C), while the experiments for intestinal fatty acid binding protein (IFABP) were recorded on samples of uniformly ^{13}C, ^{15}N-labeled protein in the presence and absence of oleic acid (∼1 mM protein, pH 7.0, 10 mM K_3PO_4, 10% D_2O, 25 °C). The oleic acid concentration in the holo-IFABP sample is ∼1.5 mM. ^{13}C R_1 data were measured with the pulse scheme shown in Figure S1 in the Supporting Information. The relaxation delays used were 10, 50, 100, 200, 300, 400, and 600 ms for UB and 10, 50, 100, 200, 300, 400, and 650 ms for IFABP. The cross-correlated relaxation rates were measured using the scheme shown in Figure 1. For UB, 16 spectra were recorded by setting the constant-time T to 84 ms with a series of Δ values: 0.012, 0.6, 1.2, 1.8, 2.4, 3.0, 3.6, 4.2, 4.8, 5.6, 6.4, 7.2, 8.0, 9.2, 21.2, and 24 ms. For IFABP, 14 spectra were recorded at a constant time of 28 ms with a series of Δ values: 0.012, 0.6, 1.2, 1.8, 2.4, 3.0, 3.6, 4.2, 4.8, 5.4, 6.0, 6.6, 7.2, and 8.0 ms. A recycle delay of 1.5 s was used in all ^{13}C experiments. ^{15}N relaxation times T_1 and $T_{1\rho}$ and $^{15}N\{^{1}H\}$ NOE were measured with well-established experiments.[32,33] The $T_{1\rho}$ experiments were done with a spin-lock field strength of 1.6 kHz and a recycle delay of 2 s. T_2 values were derived from $T_{1\rho}$ measurements after offset corrections. The ^{1}H saturation time used for $^{15}N\{^{1}H\}$ NOE development was about $10T_1$ of ^{15}N spins.

All NMR data were processed with the NMRPipe/nmrDraw software package.[34] Intensities were obtained using the nonlinear line-shape modeling procedure included in the software. The standard deviations of peak intensities were determined from measured background noise levels. R_1 values were obtained from fitting the measured peak intensities to a single-exponential equation with two parameters. Γ values were determined by fitting relative peak intensities to eqs 5 and 7, using simplex routines in MATLAB (The MathWorks Inc.). Fitting errors were calculated using the Monte Carlo method.

Extraction of Dynamic Parameters from Relaxation Data. The ^{13}C spin−lattice relaxation rate (R_1) and dipole−dipole cross-correlated relaxation rate (Γ) of a methyl group in a uniformly ^{13}C-labeled protein

(24) Lee, A. L.; Flynn, P. F.; Wand, A. J. *J. Am. Chem. Soc.* **1999**, *121*, 2891−2902.
(25) Ishima, R.; Petkova, A. P.; Louis, J. M.; Torchia, D. A. *J. Am. Chem. Soc.* **2001**, *123*, 6164−71.
(26) Liu, W. D.; Zheng, Y.; Cistola, D. P.; Yang, D. W. *J. Biomol. NMR* **2003**, *27*, 351−364.
(27) Banaszak, L.; Winter, N.; Xu, Z. H.; Bernlohr, D. A.; Cowan, S.; Jones, T. A. *Adv. Protein Chem.* **1994**, *45*, 89−151.
(28) Storch, J.; Thumser, A. E. A. *Biochim. Biophys. Acta* **2000**, *1486*, 28−44.
(29) Sacchettini, J. C.; Scapin, G.; Gopaul, D.; Gordon, J. I. *J. Biol. Chem.* **1992**, *267*, 23534−45.
(30) Hodsdon, M. E.; Cistola, D. P. *Biochemistry* **1997**, *36*, 1450−60.
(31) Hodsdon, M. E.; Cistola, D. P. *Biochemistry* **1997**, *36*, 2278−90.
(32) Farrow, N. A.; Muhandiram, R.; Singer, A. U.; Pascal, S. M.; Kay, C. M.; Gish, G.; Shoelson, S. E.; Pawson, T.; Forman-Kay, J. D.; Kay, L. E. *Biochemistry* **1994**, *33*, 5984−6003.
(33) Korzhnev, D. M.; Skrynnikov, N. R.; Millet, O.; Torchia, D. A.; Kay, L. E. *J. Am. Chem. Soc.* **2002**, *124*, 10743−53.
(34) Delaglio, F.; Grzesiek, S.; Vuister, G. W.; Zhu, G.; Pfeifer, J.; Bax, A. *J. Biomol. NMR* **1995**, *6*, 277−293.

are dominated by $^{13}C-^{1}H$ dipolar interactions and given by[26]

$$R_1 \approx 3\frac{\hbar^2\gamma_C^2\gamma_H^2}{10r_{CH}^6}\left(\frac{\mu_0}{4\pi}\right)^2[J(\omega_H-\omega_C)+3J(\omega_C)+6J(\omega_H+\omega_C)]+ \frac{\hbar^2\gamma_C^4}{10r_{CC}^6}\left(\frac{\mu_0}{4\pi}\right)^2[J(0)+3J(\omega_C)+6J(2\omega_C)]+\frac{2\omega_C^2\Delta\sigma^2}{15}J(\omega_C) \quad (1)$$

$$\Gamma = \frac{\hbar^2\gamma_H^2\gamma_C^2}{10r_{CH}^6}\left(\frac{\mu_0}{4\pi}\right)^2[4J_{HCH}(0)+3J_{HCH}(\omega_C)]+ \frac{\hbar^2\gamma_H^4}{10r_{HH}^6}\left(\frac{\mu_0}{4\pi}\right)^2[3J_{HHH}(\omega_H)+3J(2\omega_H)] \quad (2)$$

in which γ_i and ω_i are the gyromagnetic ratio and Lamor frequency of spin i, respectively; $\hbar = h/2\pi$ and h is Planck's constant; μ_0 is the permittivity of free space; $\Delta\sigma = \sigma_{||} - \sigma_{\perp}$, where $\sigma_{||}$ and $\sigma_{\perp}$ are the principle components of an axially symmetric ^{13}C CSA tensor along the parallel and perpendicular axes, and $\Delta\sigma$ is assumed as 25 ppm; r_{CH} is the C−H bond distance and is assumed as 1.115 Å; r_{CC} is the C−C bond distance assumed as 1.517 Å; r_{HH} is the distance between two protons in the methyl group, and it is 1.821 Å when a tetrahedral geometry is assumed; $J(\omega)$ and $J_{HCH}(\omega)/J_{HHH}(\omega)$ are autocorrelation and cross-correlation spectral density functions, respectively.

As a result of steric constraints and concerted motions, the dynamics of methyl groups in protein are complicated, especially for Leu and Ile, and a detailed picture of the dynamics cannot be obtained merely from a few experimental data. The simplest approach to extract meaningful dynamic parameters from relaxation data is the Lipari−Szabo (LS) model-free analysis.[35,36] Assuming that the overall tumbling of protein is isotropic, the model-free form of the spectral density function is described by

$$J_{ijk}(\omega) = \frac{S_f^2 S_{axis}^2\tau_m}{1+\omega^2\tau_m^2} + \frac{(P_2(\theta_{ij,jk}) - S_{axis}^2 S_f^2)\tau_1}{1+\omega^2{\tau_1}^2} \quad (3)$$

where S_{axis} is the order parameter of the methyl rotation axis; $S_f^2 = P_2(\cos(\theta_{ij}))*P_2(\cos(\theta_{jk}))$, θ_{ij} is the angle between bond ij and the rotation axis, and both bonds ij and jk undergo free rotation about the rotation axis; for CH_3 methyl groups, $\theta_{CH} = 110.5°$, while $\theta_{CD} = 109.5°$ for CH_2D methyl groups;[25] ${\tau_1}^{-1} = {\tau_m}^{-1} + {\tau_e}^{-1}$, in which τ_m is the correlation time for overall molecular tumbling, τ_e is the effective internal correlation time and $\tau_m > 10\tau_e$; $\theta_{ij,jk}$ is the angle between bonds ij and jk. In the case where $ij = jk$, $J_{ijk}(\omega)$ is the autocorrelation spectral density function and is denoted as $J(\omega)$.

More complicated approaches such as extended LS models with more motional parameters can be applied to describe methyl dynamics with multiple internal motions.[37] However, recent studies have shown that the motional parameters for methyl groups extracted from use of the extended LS models are significantly influenced by small errors in relaxation data (e.g., as small as ~3%), even in cases where extensive data sets at four static fields are used.[38] This is because $J(\omega)$ is insensitive to methyl motions on subnanoseconds and nanoseconds. To take account of the effect of overall anisotropic tumbling on methyl relaxation, precise side-chain geometry (which is available if high-resolution structures are already determined) and more experimental data sets are required for extracting meaningful dynamics parameters since methyl groups undergo multiple restricted rotations about $\chi_1-\chi_N$ torsion angles. Therefore, we only use the simplest model (eq 3) to extract order parameters and effective internal correlation times.

Both R_1 and Γ are dominated by one-bond $^{1}H-^{13}C$ dipolar interactions. In extreme cases, however, the contributions of $^{13}C-^{13}C$ and $^{1}H-^{1}H$ dipolar relaxations to respective R_1 and Γ can be significant and cannot be neglected as shown by our numerical simulations. For example, the contribution of $^{13}C-^{13}C$ dipolar interaction to R_1 is >25% in the cases where $S^2 > 0.95$, $\tau_f < 3$ ps, $\tau_m = 8$ ns, and $\omega_H = 800$ MHz. This contribution increases with τ_m and S^2 but dramatically decreases with the increase of τ_f ($0 < \tau_f < 110$ ps). The contribution of $^{1}H-^{1}H$ dipolar relaxation to Γ can be >15% in cases where $S^2 < 0.2$, $\tau_f > 100$ ps, $\tau_m = 8$ ns, and $\omega_H = 800$ MHz. This contribution increases with τ_f ($0 < \tau_f < 110$ ps) but decreases with the increase of τ_m and S^2. The total contribution of all ^{13}C dipolar interactions with remote ^{1}Hs to R_1 is always smaller than 2% as estimated from proton−carbon distances in a number of proteins, while the remote $^{1}H-^{13}C$ and $^{1}H-^{1}H$ dipolar interactions have negligible effects on Γ.

Heteronuclear steady-state NOEs are commonly used for dynamics studies. However, $^{13}C\{^{1}H\}$ NOEs in uniformly ^{13}C-labeled proteins are complicated by $^{13}C-^{13}C$ cross-relaxation effects. Our numerical simulations indicated that the contribution from cross-relaxation to measured methyl NOE values can be as large as up to 7% for methyl groups in proteins with a τ_m value of 10 ns (Figure S2 in the Supporting Information). The contribution increases greatly with the increase in protein size (e.g., up to 14% when $\tau_m = 15$ ns) and is difficult to predict without prior knowledge of the dynamics at the sites adjacent to methyl groups. Moreover, R_1 and NOE contain redundant information as both R_1 and NOE are sensitive to fast motions. Therefore, NOE values were not measured in this study.

Results and Discussion

Measurement of ^{13}C Spin−Lattice Relaxation Rate. The previous pulse schemes for measuring methyl ^{13}C R_1 values record the ^{13}C chemical shift after the relaxation period.[24,39] It has been shown that the R_1 values measured in this manner are dependent on the initial magnetization of the carbon spins adjacent to methyl groups and equivalent to nonselective relaxation rates.[40] Differences in dynamics at the sites adjacent to methyl groups will complicate the extraction of accurate relaxation rates. If the ^{13}C chemical shift is recorded prior to the relaxation period (Figure S1 in the Supporting Information), R_1 values not only are equivalent to selective relaxation rates but also can be accurately measured for small proteins by fitting the experimental data to a single exponential.

Our numerical simulations showed that errors in R_1 values are less than 2.5% for proteins with an overall correlation time (τ_m) of 8 ns when they are measured with the scheme shown in Figure S1 on an 800 MHz spectrometer. The errors are caused by $^{13}C-^{13}C$ cross-relaxation effects. The relative error ($\delta R_1/R_1$, δR_1 is the difference of the theoretical and measured R_1 values) decreases dramatically as internal correlation time (τ_e) increases (e.g., <1.5% when $\tau_e > 0.01$ ns), but it increases significantly as τ_m increases since R_1 and δR_1 are dominated by $(1 - S_f^2 S_{axis}^2)\tau_e$ and $S_{axis}^2\tau_m$, respectively (Figure S3). The error can be as large as 8% for methyl groups in proteins with a τ_m value of 15 ns, while it is smaller than 0.4% for proteins the size of UB. If the experiment is performed at lower magnetic fields, the error in R_1 is even smaller.

Measurement of Methyl Dipole−Dipole Cross-Correlated Relaxation Rate. Figure 1 shows the pulse scheme used to

(35) Lipari, G.; Szabo, A. *J. Am. Chem. Soc.* **1982**, *104*, 4546−4559.
(36) Lipari, G.; Szabo, A. *J. Am. Chem. Soc.* **1982**, *104*, 4559−4570.
(37) Clore, G. M.; Szabo, A.; Bax, A.; Kay, L. E.; Driscoll, P. C.; Gronenborn, A. M. *J. Am. Chem. Soc.* **1990**, *112*, 4989−4991.
(38) Choy, W. Y.; Zhou, Z.; Bai, Y.; Kay, L. E. *J. Am. Chem. Soc.* **2005**, *127*, 5066−72.
(39) Nicholson, L. K.; Kay, L. E.; Baldisseri, D. M.; Arango, J.; Young, P. E.; Bax, A.; Torchia, D. A. *Biochemistry* **1992**, *31*, 5253−63.
(40) Yamazaki, T.; Muhandiram, D. R.; Kay, L. E. *J. Am. Chem. Soc.* **1994**, *116*, 8266−78.

measure methyl dipole−dipole cross-correlated relaxation. The scheme is similar to the standard constant-time HSQC sequence. The composite ^{1}H 180° pulse applied in the middle of the constant-time period (T) suppresses the cross-correlation between ^{1}H−^{13}C dipolar and ^{13}C CSA interactions. The removal of ^{13}C−^{13}C coupling effects is achieved by applying a constant-time acquisition mode. The maximum chemical shift evolution time for ^{13}C spins equals $T-\Delta$. In the absence of relaxation, the observed methyl signal intensity is a function of delay Δ and is given by $3\cos(3\pi J\Delta) + \cos(\pi J\Delta)$, where J is the one-bond ^{13}C−^{1}H coupling constant. In the presence of relaxation, the signal intensity cannot be precisely described by a simple analytical form due to cross-correlated interactions within a methyl group and cross-relaxation between the methyl and its proximal protons. Nevertheless, when $2\pi J \gg 1.5R_{1\mathrm{Hsel}}$, where $R_{1\mathrm{Hsel}}$ is the selective longitudinal relaxation rate of methyl protons, the dependence of the signal intensity on delays Δ and T can be approximated as[26,41]

$$I'(\Delta,T) = 0.75\cos(3\pi J\Delta)\exp(-R_{\mathrm{out}}T)[\exp(-2\tau_a R_f) + \exp(-2\tau_a R_s)] \times [\exp(-(2\tau_b + t_{\mathrm{aq}})R_f) + \exp(-(2\tau_b + t_{\mathrm{aq}})R_s)] + 0.25\cos(\pi J\Delta)\exp(-R_{in}T)\{[-\exp(-2\tau_a R_f) + 3\exp(-2\tau_a R_s)]\exp[-(2\tau_b + t_{\mathrm{aq}})R_s] + [3\exp(-2\tau_a R_f) - \exp(-2\tau_a R_s)]\exp[-(2\tau_b + t_{\mathrm{aq}})R_f]\} \quad (4)$$

where R_{out} is the average relaxation rate of the two outer lines of the ^{13}C quartet; R_{in} is the average relaxation rate of the two inner lines; R_f is the relaxation rate of the proton magnetization involved in $^3/_2 \rightarrow {}^1/_2$ and $-{}^1/_2 \rightarrow -{}^3/_2$ transitions; R_s is the relaxation rate of the proton magnetization involved in $^1/_2 \rightarrow -{}^1/_2$ transitions; R_f is dominated by dipolar ^{1}H−^{1}H interactions within the methyl group, while R_s is governed by dipolar ^{1}H−^{1}H interactions between the methyl and its proximal protons ($R_{2\mathrm{Hext}}$);[41] t_{aq} is the acquisition time in the direct detection dimension. The ratio of the methyl signal intensity at delay Δ with respect to that at a delay time of zero (i.e., relative intensity, $I'(\Delta,T)/I'(0,T)$) can be written as

$$I(\Delta,T) = \frac{3\cos(3\pi J\Delta)\exp(-4\Gamma T) + (1+x)\cos(\pi J\Delta)}{3\exp(-4\Gamma T) + (1+x)} \quad (5)$$

where Γ is the methyl dipole−dipole cross-correlated relaxation rate given by eq 2, and x is given by

$$x = \frac{2[\exp(-2\tau_a R_s) - \exp(-2\tau_a R_f)]}{[\exp(-2\tau_a R_s) + \exp(-2\tau_a R_f)]} \times \frac{[\exp(-2\tau_b R_s)(1-\exp(-R_s t_{\mathrm{aq}}))/R_s - \exp(-2\tau_b R_f)(1-\exp(-R_f t_{\mathrm{aq}})/R_f)]}{[\exp(-2\tau_b R_s)(1-\exp(-R_s t_{\mathrm{aq}}))/R_s + \exp(-2\tau_b R_f)(1-\exp(-R_f t_{\mathrm{aq}})/R_f)]} \quad (6)$$

R_s and R_f are dependent on τ_{m}, S^2_{axis}, $R_{2\mathrm{Hext}}$, and τ_{e}, and so is x. Both R_s and R_f can be approximately expressed with Γ and $R_{2\mathrm{Hext}}$. For proteins, $R_{2\mathrm{Hext}} \approx 2.5R_{1\mathrm{Hsel}}$.[26] $R_{1\mathrm{Hsel}}$ was found to be in the range $0.4\tau_{\mathrm{m}}-1.2\tau_{\mathrm{m}}$ s^{-1} for UB and IFABP, where τ_{m} is the overall tumbling time of a given protein in nanoseconds. To simplify data analysis, it is better to roughly express x as a function of Γ and τ_{m}. When $\tau_{\mathrm{a}} = 0.001$ s, $\tau_{\mathrm{b}} = 0.00195$ s, $t_{\mathrm{aq}} = 0.057$ s, and $R_{2\mathrm{Hext}} = 2\tau_{\mathrm{m}}$ s^{-1}, our numerical simulations indicate that x can be approximated as

$$x \approx 15\tau_a\Gamma \times [1 - \exp(-y\Gamma)] \quad (7a)$$

$$y = 0.2229 - 0.0046\tau_{\mathrm{m}} + 0.000052\tau_{\mathrm{m}}^2 \quad (7b)$$

where τ_a, τ_{m}, and Γ are expressed in units of s, ns, and s^{-1}. To obtain maximum experimental sensitivity, τ_{a} should be set to $1/(4J)$ (~2 ms). To reduce the value of factor x; however, it was set to 1 ms in our measurements. Figure S4 in the Supporting Information shows the excellent agreement between eqs 6 and 7 (comparison of $1 + x$). For small proteins such as UB with a τ_{m} value of 4.1 ns, the maximum value of x is ~0.02 and the effect of x on $I(\Delta,T)$ is negligible. Simulations indicate that the effects of τ_{e} and ω_{H} on x are negligible since R_f and R_s are dominated by $J(0)$. Simulations also show that x is insensitive to the exact value of $R_{2\mathrm{Hext}}$ when $R_{1\mathrm{Hsel}}$ is within the range $0.4\tau_{\mathrm{m}}-1.2\tau_{\mathrm{m}}$ s^{-1}. For example, the maximum value of x equals ~0.064 when $R_{2\mathrm{Hext}} = 2.5{*}0.4\tau_{\mathrm{m}}$ s$^{-1} = 8$ s^{-1}, while $x = 0.057$ when $R_{2\mathrm{Hext}} = 2.5{*}1.2\tau_{\mathrm{m}}$ s$^{-1} = 24$ s^{-1}. Equation 7b is valid only when $\tau_{\mathrm{a}} = 0.001$ s, $\tau_{\mathrm{b}} = 0.001\,95$ s, and $t_{\mathrm{aq}} = 0.057$ s. If another set of delays is used, x and y can be calculated from an MATLAB script freely available at http://yangdw.science.nus.edu.sg. Therefore, the cross-correlation rate, Γ, can be obtained from dependence of the relative intensity ratio ($I(\Delta, T)$) on delay Δ at a given constant-time T based on eqs 5 and 7.

In this paper, we only analyze the time course of the magnetization evolution to obtain the cross-correlation rate. Alternatively, one can use a third dimension to record a quaternary structure for each methyl group by varying Δ systematically with the same pulse scheme shown in Figure 1. Note that chemical shifts are removed in the third dimension, and acquisition of a few points in this dimension is sufficient to resolve the quaternary structure. The cross-correlation rate can be obtained by analyzing the line shape of each multiplet component (or peak intensity ratio) in the frequency domain.

Figure 2 shows the representative profiles of relative peak intensities for L8δ2, T9γ, V26γ2, and A46β methyl groups in UB. Due to one-bond ^{1}H−^{13}C J coupling interaction, the change of the peak intensity with delay Δ follows a simple form, $0.75\cos(3\pi J\Delta) + 0.25\cos(\pi J\Delta)$, shown as dotted lines in Figure 2. Deviation from this profile indicates the presence of cross-correlated relaxation. Dipole−dipole cross-correlated relaxation rates and J coupling constants were determined by fitting the relative peak intensity profiles to eqs 5 and 7 under the condition $\tau_{\mathrm{m}} = 4.1$ ns (τ_{m} was determined from ^{15}N relaxation times T_1 and T_2). The best fits are indicated by solid lines, and they reproduce the measured peak intensities very well. Since the HSQC-type experiment is very sensitive, high accuracy in the intensity ratios is easily achievable. Thus J and Γ values can be measured accurately with this experiment. In the case where the chemical shift difference between Cδ and Cγ spins in a Leu residue is not much larger than the one-bond ^{13}C−^{13}C coupling constant (i.e., $|\sigma_{\mathrm{C}}\delta - \sigma_{\mathrm{C}}\gamma| < 12J_{\mathrm{CC}}$), the strongly coupled ^{13}C−^{13}C interaction interferes with the weakly coupled ^{1}H−^{13}C interaction (or the Hamiltonians corresponding to the two interactions do not commute). For such a Leu methyl group, its peak intensity profile can deviate from eq 5 significantly. In this case, J and Γ values could not be obtained reliably. Due to

(41) Tugarinov, V.; Hwang, P. M.; Ollerenshaw, J. E.; Kay, L. E. *J. Am. Chem. Soc.* **2003**, *125*, 10420−8.

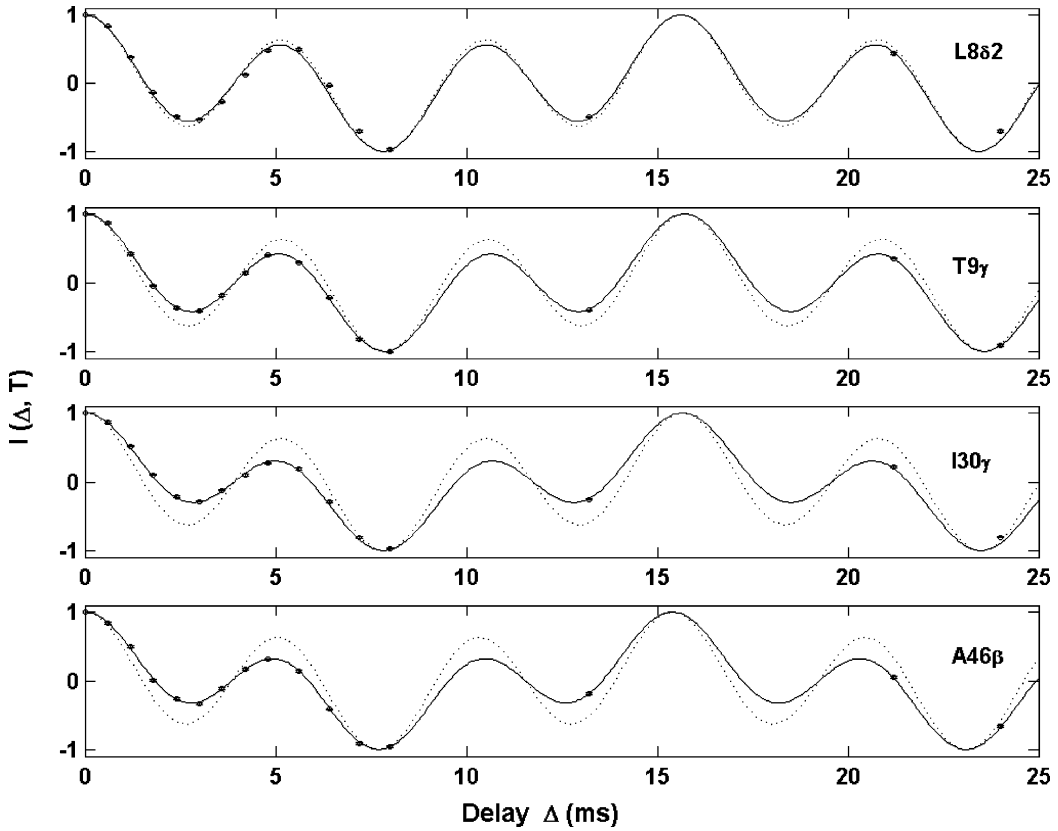

Figure 2. Time dependence of the relative peak intensities of a number of representative methyl groups in ubiquitin, which is caused by the one-bond ^{1}H-^{13}C coupling and dipole−dipole cross-correlated relaxation. The data were recorded with a constant-time T of 84 ms. Experimental data are indicated by symbol "o". The experimental errors in intensities are shown in vertical bars which were often smaller than 1% and thus are within the symbol. The solid lines represent the curves with the best fit using eqs 5 and 7 and assuming $\tau_m = 4.1$ ns. The dotted lines correspond with the predicted curves in the absence of cross-correlated relaxation. The J_{CH} coupling constants (fitting errors) for L8δ2, T9γ, I30γ, and A46β methyls are 128.1 (0.1), 127.3 (0.1), 127.8 (0.1), and 129.9 (0.1) Hz. The values of Γ are listed in Table S1.

the strong coupling effect, five Leu methyl groups (L15δ1, L50δ1, L56δ1 and L56δ2, L69δ1) in UB were excluded for analysis. Five methyl groups were not resolved in the HSQC spectrum and thus could not be measured. In total, the cross-correlated relaxation rates for 39 out of 49 methyl groups were obtained. Several Leu methyl groups had relatively large uncertainties in J and Γ because the spins under investigation do not form a rigorously weakly coupled spin-system.

Extraction of Dynamic Parameters. The dynamic parameters (S^2_{axis} and τ_e) were determined by fitting T_1 and Γ data to eqs 1−3, assuming $r_{CH} = 1.115$ Å and $\theta_{CH} = 110.5°$, where θ_{CH} is the angle between the CH bond and the methyl rotation axis.[25] The error in T_1 mainly resulting from $^{13}C-^{13}C$ cross-relaxation only influences the accuracy of τ_e. It has nearly no effect on the determination of side-chain mobility (S^2_{axis}), which is dominated by Γ.[26] Unlike T_2 or $T_1\rho$, Γ is free of chemical exchange contributions. Therefore, the determination and interpretation of S^2_{axis} with this method are not complicated by slow motions on microsecond-to-millisecond time scales. Figure 3 shows the comparisons of S^2_{axis} and τ_e values derived from ^{13}C and ^{2}H relaxation data. The dynamic parameters measured using ^{2}H relaxation times were taken from Wand's work in which the angle θ_{CD} was assumed to be 109.5°.[24] The correlation between S^2_{axis} values is excellent. The small deviations might have arisen from experimental errors and a difference in sample condition. The τ_e values (dominated by T_1) derived from ^{13}C relaxation data are ∼10% smaller than those from ^{2}H relaxation times. The difference might have resulted from the fact that ^{2}H T_1 is slightly more sensitive to slower motions than ^{13}C T_1. A similar discrepancy was also observed for the effective correlation times derived from ^{13}C and ^{2}H relaxation times that were measured with the respective CHD_2 and CH_2D isotopomers in the same sample,[25] provided that $\theta_H = 110.5°$ and $\theta_D = 109.5°$. The good agreement between the two sets of data indicates that methyl dynamics can be probed using ^{13}C T_1 and $^{13}C-^{1}H$ dipolar cross-correlated relaxation data.

Application to Human IFABP. For rat IFABP, it was found that the portal region is more dynamic on the millisecond-to-microsecond time scale in the absence than in the presence of a ligand based on amide exchange and backbone ^{15}N relaxation times.[31] Because most residues in the portal region undergo conformational exchanges which contribute to relaxation time T_2 significantly, their order parameters, characterizing mobility on the nanosecond-to-picosecond time scale, cannot be accurately measured. In this case, heteronuclear $^{15}N\{^{1}H\}$ NOEs can be used to characterize dynamics differences in fast motions. A comparison of $^{15}N\{^{1}H\}$ NOEs of human apo- and holo-IFABPs is shown in Figure 4. Clearly, the second helix (residues 25−32) is slightly more flexible than other parts of the protein on the nanosecond-to-picosecond time scale. However, there is no difference in fast motions between the apo- and holo-forms within experimental errors.

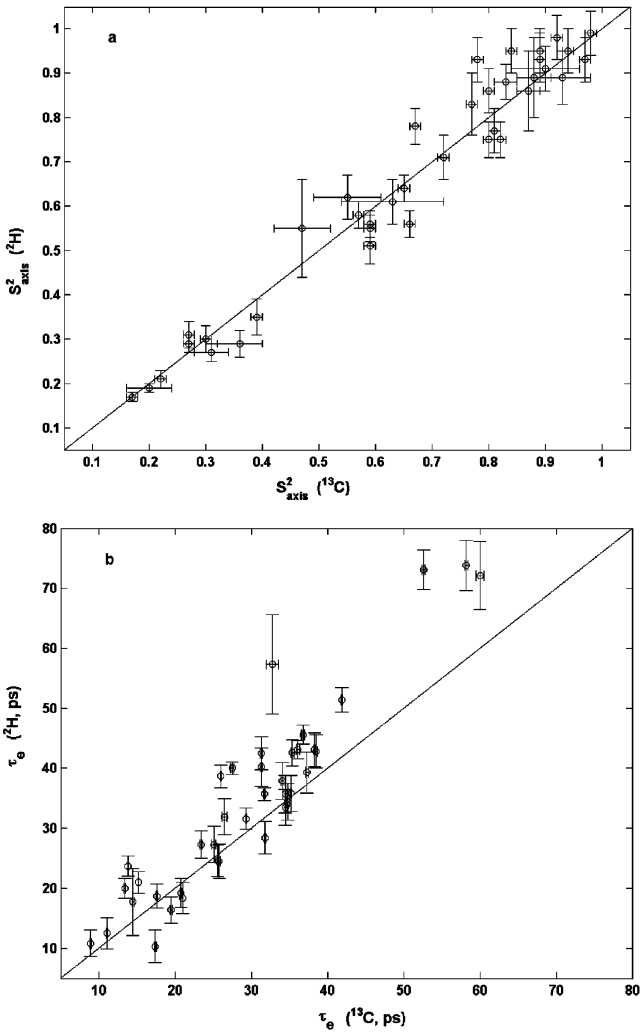

Figure 3. Comparison of order parameters (S^2_{axis}, a) and internal effective correlation times (τ_e, b) determined from ^{13}C T_1's and methyl dipole−dipole cross-correlated relaxation rates versus the values determined from ^{2}H relaxation times T_1 and T_2. The S^2_{axis} and τ_e values from ^{2}H measurements were taken from a previous published paper.[24]

Since the backbone may not participate in direct interactions with a fatty acid, side chains must interact directly with the ligand. To investigate the effect of fatty acid binding on side chains, we applied the method shown above for probing methyl dynamics of human IFABP in the presence and absence of oleic fatty acid using uniformly ^{13}C-, ^{15}N-labeled proteins. Figure 5 shows the intensity profiles of a couple of methyl groups of IFABP in the presence and absence of oleic acid. Cross-correlated relaxation rates were obtained by fitting the intensities to eqs 5 and 7 under the condition of $\tau_m = 8.2$ ns. Γ values obtained here are consistent with those measured using a TOCSY-based experiment,[26] but they are more accurate because the HSQC-based experiment is much more sensitive than the TOCSY-based one. Using methyl ^{13}C T_1 and Γ data, methyl dynamics parameters were obtained with an isotropic overall tumbling time of 8.2 ns for both apo- and holo-forms. The overall tumbling time was calculated from ^{15}N relaxation times T_1 and T_2. The dynamic parameters for 46 and 48 out of 74 methyl groups were obtained for apo- and holo-forms, respectively (Tables S2 and S3 in the Supporting Information), while the dynamic parameters were available for only 37 methyl groups in both forms. Ten Leu methyl groups were excluded for analysis due to the strong coupling effect mentioned above. Eighteen and 16 methyl groups were not resolved in the ^{13}C-^{1}H HSQC spectra of apo- and holo-IFABPs, respectively. Thus they were excluded for extracting dynamics data.

Many methyl groups show small but significant increases in order parameters upon oleic acid binding to IFABP. Figure 6 shows changes of methyl S^2_{axis} values. Methyl groups located in the portal region (M18, M21, V23, I25, V26, L30, A31, A32, A54, and A73) become more rigid in the presence of the ligand. This is consistent with structural changes in solution as observed for rat IFABP;[30] i.e., the binding of oleate to IFABP increases the helical content of the second α-helix and the order of the flexible ligand entry portal. Note that human and rat IFABPs have very high sequence homology (81% in identity and 90% in similarity). In the absence of fatty acid, M18Cϵ is quite flexible with an S^2_{axis} value of 0.3. On the other hand, it becomes very rigid with an S^2_{axis} value of 0.94 in the presence of a fatty acid. According to the solution structure of the holo-form,[42] the methyl group of M18 interacts with a number of residues in β-turns in the portal region (Y14 and M21 in the first helix, V23 between two helices, and A31 in the second helix) in the presence of a fatty acid. Although no structure is available for the apo-form of human IFABP, the dramatic change of S^2_{axis} for M18 indicates that many of the hydrophobic interactions involved in the holo-form do not exist in the apo-form (i.e., the portal region is less ordered in the apo-form on the nanosecond-to-picosecond time scale). The methyl group of M21 is located in a less compact region in the holo-form. Thus its S^2_{axis} is much smaller than that for M18. A much smaller increase in the S^2_{axis} ($\sim$0.09) of M21 induced by fatty acid binding implies no major difference in side-chain arrangement around the methyl group of M21 between the apo- and holo-forms. Interestingly, M18 is conserved among all human fatty acid binding proteins, but M21 is not. This conserved Met may play an important role in regulating the binding affinity of fatty acids to proteins.

Although the exact ligand binding site is unknown for human IFABP, intermolecular ^{1}H−^{1}H NOEs (unpublished data) indicate that M18, M21, V23, and A73 interact with the methyl group of the fatty acid; V60 and W82 interact with the middle part and carboxyl end of the ligand, respectively. W82 is in contact with R106. R106 is a conserved residue for intestinal FABPs, found to form hydrogen bonds with the carboxyl group of the fatty acid. The residues located in the ligand binding region (I58 and V60 are close to each other; I40 and L113 are in one cluster close to R106) become more rigid upon formation of a protein−ligand complex. This reduction in methyl mobility arises from van der Waals interactions between methyl side chains and the fatty acid. A number of methyl groups (V8, I90, I108, I109, and I127) that are far away from the binding sites also show increases in S^2_{axis} when IFABP binds to a fatty acid. This may result from changes of side-chain orientations instead of mobility[17] or from long-range conformational couplings to the residues in the binding regions.[43] A couple of methyl groups

(42) Zhang, F. L.; Lucke, C.; Baier, L. J.; Sacchettini, J. C.; Hamilton, J. A. *J. Biomol. NMR* **1997**, *9*, 213−228.
(43) Millet, O.; Mittermaier, A.; Baker, D.; Kay, L. E. *J. Mol. Biol.* **2003**, *329*, 551−563.

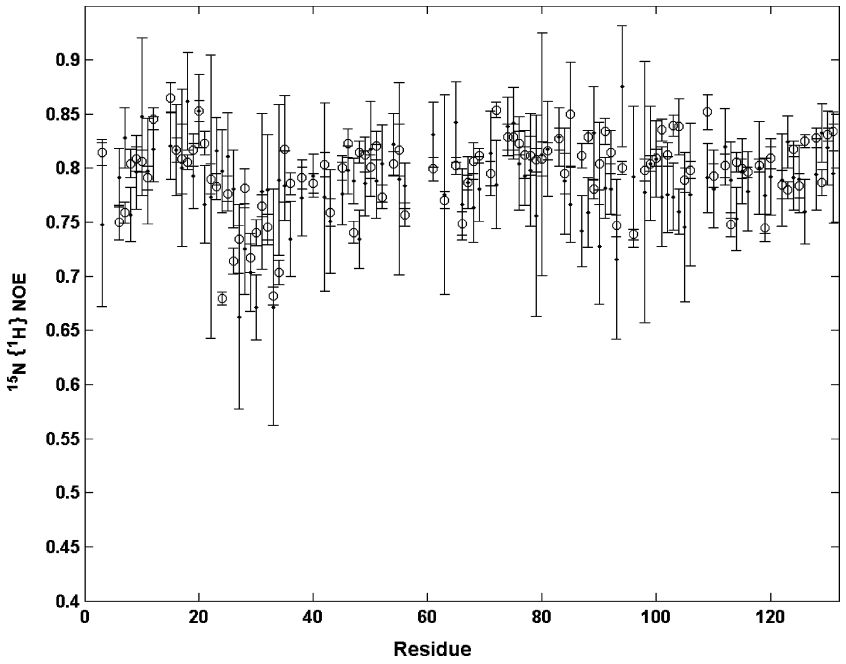

Figure 4. Plot of heteronuclear $^{15}N\{^1H\}$ NOE as a function of residue number for apo- (○) and holo- (●) IFABP. Uncertainties in NOEs are indicated with vertical bars.

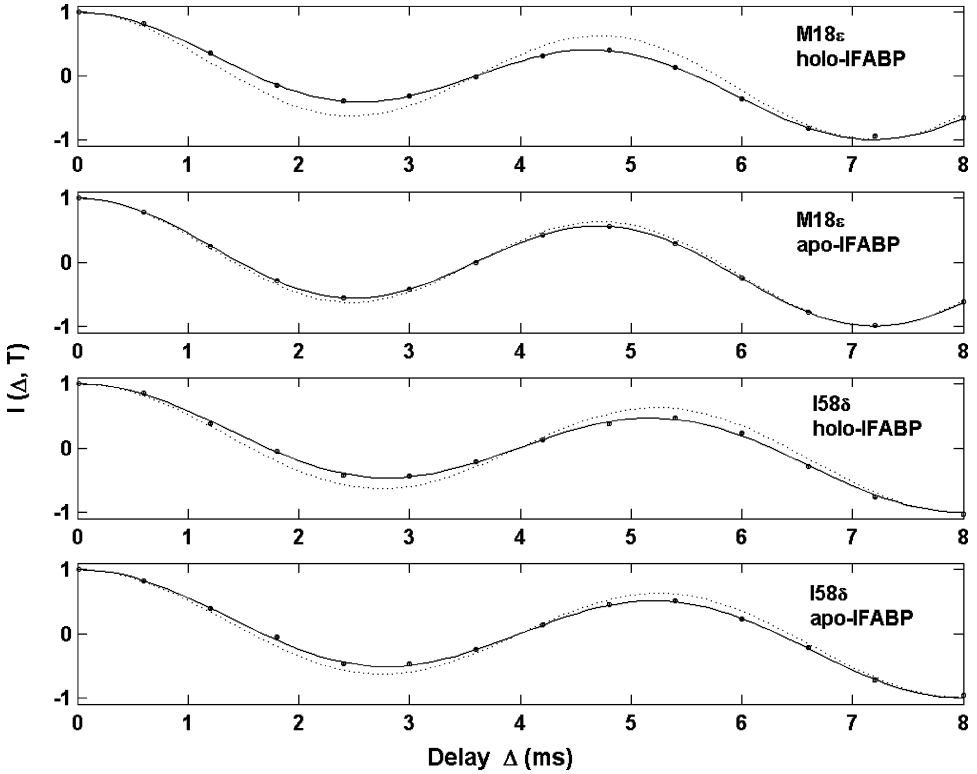

Figure 5. Profiles of relative peak intensities of representative methyl groups in both apo- and holo-IFABPs. The data were recorded with a constant-time T of 28 ms. Experimental data are indicated by symbol "○". The experimental errors in intensities are shown in vertical bars. The solid lines represent the curves with the best fit using eqs 5 and 7 and assuming $\tau_m = 8.2$ ns. The dotted lines correspond to the predicted curves in the absence of cross-correlated relaxation.

(T48 and V89) have smaller S^2_{axis} values in the holo-form than apo-form. In addition, several methyl groups (T41,V66, T67, T76, T81, V105, and V114) that are not resolved in the $^{13}C-^1H$ HSQC spectra of the apo- or/and holo-IFABP display decreased S^2_{axis} upon oleic acid binding to IFABP as shown by 3D TOCSY-based experiments (unpublished data).[26] This might be caused by increases in mobility, side-chain orientation changes, or the long-range conformational couplings.

Concluding Remarks

In summary, we have described a simple method for probing methyl dynamics from dipole−dipole cross-correlated relaxation

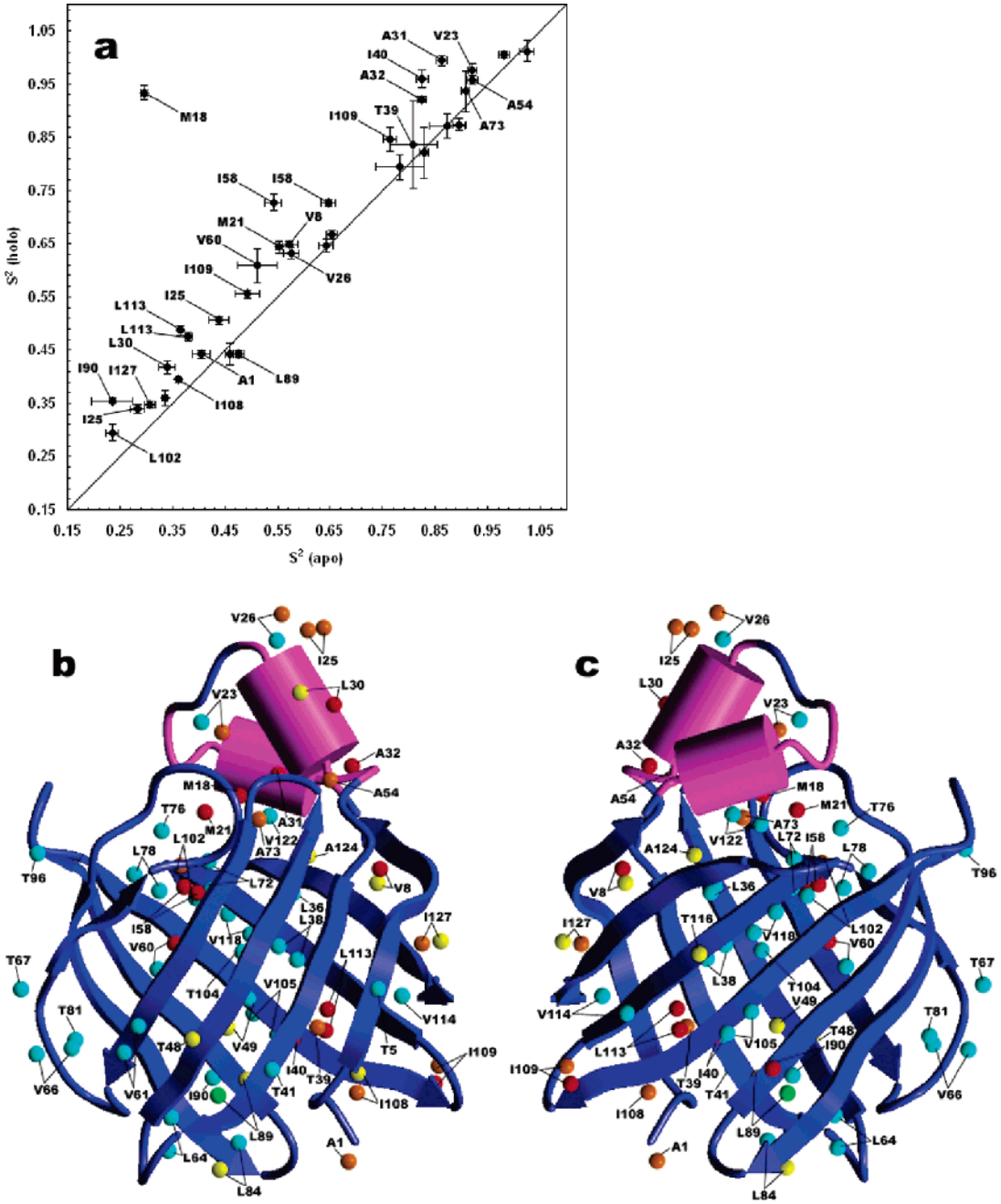

Figure 6. (a) Plot of S^2_{axis}(apo) versus S^2_{axis}(holo). Only the methyls with significant differences in order parameters ($\Delta S^2_{axis} = S^2_{axis}$(holo) $- S^2_{axis}$(apo), larger than 0.025 or smaller than −0.025) are labeled. (b, c). ΔS^2_{axis} values are mapped onto the solution structure of human IFABP in the presence of a fatty acid. The backbone is shown as a ribbon diagram. Methyl carbons are shown in a space-filling representation. Methyl groups for which no ΔS^2_{axis} data could be obtained for both apo- and holo-IFABPs are shown in cyan. The remaining methyl groups are color-coded as follows: $\Delta S^2_{axis} \geq 0.075$ (red); $0.025 \leq \Delta S^2_{axis} < 0.075$ (orange); $-0.025 < \Delta S^2_{axis} < 0.025$ (yellow); $\Delta S^2_{axis} \leq -0.025$ (green). Panel c presents the back view of the structure as shown in panel b.

and ^{13}C spin−lattice relaxation. The method has been demonstrated on a sample of ubiquitin and applied to obtain side-chain dynamics changes of human fatty acid binding protein upon ligand binding. Although apo- and holo-IFABPs show very similar backbone dynamics on a nanosecond-to-picosecond time scale, methyl dynamics reveal that side chains in the portal region and binding sites become more rigid upon formation of a protein−ligand complex. Unlike TOCSY-based experiments, the method presented here is suitable for both small and large proteins because of the high sensitivity of the 2D HSQC-based experiment. The consistency of order parameters obtained from ^{2}H autorelaxation and ^{13}C cross-correlated relaxation shows that methyl dynamics on a nanosecond-to-picosecond time scale can be easily obtained from methyl CH_3 T_1 and Γ using the same sample as in structural determination (i.e., ^{13}C-, ^{15}N-labeled proteins).

Acknowledgment. This research was supported by the National University of Singapore Natural Science Foundation of China (NSFC 20610104). The authors thank Professor D. P. Cistola (Washington University) for the sample of human intestinal fatty acid binding protein.

Supporting Information Available: One figure depicting the pulse sequence for the measurement of methyl ^{13}C R_1, two figures showing the influence of $^{13}C-^{13}C$ cross-relaxation on the measurements of methyl ^{13}C R_1 and NOE, three tables listing the dynamic parameters and relaxation data of methyl groups in UB and IFABP. This material is available free of charge via the Internet at http://pubs.acs.org.

JA057579R